

Investigating the impact of vaccination on COVID-19 dynamics and resurgence risks

Abdulaziz Y.A. Mukhtar  , Esther Ncube  and Kailash C. Patidar 

Department of Mathematics and Applied Mathematics, University of the Western Cape, Private Bag X17, Bellville, 7535, South Africa

Received February 10, 2025, Accepted July 14, 2025, Published July 24, 2025


Abstract. COVID-19 emerged in December 2019 and became a global threat, prompting heightened global surveillance from 2020 to 2022. Although COVID-19 continues to circulate and evolve, global surveillance has substantially reduced. The reduction in surveillance came after the introduction of vaccines worldwide. We formulated a mathematical model to investigate how incorporating vaccines impacts the dynamics of COVID-19 transmission. The study qualitatively analyzed the model and calculated the basic reproduction numbers (\mathcal{R}_0). We estimated the model's parameters by fitting the model to real COVID-19 case data and using maximum likelihood estimation. To determine which parameters have the greatest impact on the spread and transmission of disease, a sensitivity analysis is carried out. The analysis revealed that the transmission rate β is the most important factor responsible for the spread of COVID-19, while the vaccination rate ν has the most significant impact on controlling the disease. The numerical simulations showed that a high vaccination rate significantly reduces exposed, asymptomatic, symptomatic, and hospitalized individuals, reducing the impact of the virus on the community. It is crucial to consider the rate of immunity loss, as neglecting it could negate the benefits of vaccination.

Keywords: COVID-19, mathematical modelling, vaccination, reproduction number, sensitivity analysis.

2020 Mathematics Subject Classification: 34D20, 34D23 34C60, 92B05, 92D30.
MSC2020

1 Introduction

As of 31 March 2024, over 774 million confirmed COVID-19 cases and more than seven million deaths had been reported worldwide. COVID-19 is caused by severe acute respiratory syndrome coronavirus 2 (SARS-CoV-2). Now in its fourth year, COVID-19 continues to circulate and evolve. Millions continue to become infected or reinfected with SARS-CoV-2 despite reduced surveillance, and tragically, thousands continue to die globally [29]. This situation

 Corresponding author. Email: mukhtar982@gmail.com

necessitates long-term prevention, control, and management strategies. Surveillance has declined, with many countries ceasing to report COVID-19 cases; only 42% of countries reported between February and March 2024. Nevertheless, new cases and deaths have fallen sharply since vaccines were introduced [29].

COVID-19 spread rapidly across borders, creating an urgent threat that required immediate interventions. Governments introduced several non-pharmaceutical interventions to break the chain of transmission [24]. While COVID-19 is primarily a respiratory illness, it can also damage other vital organs, such as the heart, even though the virus does not directly infect heart tissue. The immune response triggered by infection can cause serious inflammation throughout the body [13]. The disease poses the greatest risk to the elderly and those with pre-existing health conditions, although severe illness can also occur in newborns and healthy individuals. The outbreak of COVID-19 led to the rapid development of vaccines to fight the virus. Multiple research teams and pharmaceutical companies rose to the challenge, with many collaborating to develop vaccines against SARS-CoV-2 [26]. Initial vaccination strategies prioritised individuals at high risk of complications, primarily the elderly over 65 years and key workers, before later including the remaining adult population and children. As the vaccines did not provide complete protection, booster shots were administered to maintain high levels of immunity against waning vaccine efficacy [26]. However, no COVID-19 vaccines are currently available for infants under six months old [3, 11]. The introduction of vaccines as a major pharmaceutical intervention led to a substantial decline in COVID-19-associated hospitalisations and deaths since March 2021 [5, 10, 21].

Experts have formulated mathematical models to understand disease transmission dynamics in the context of vaccination. According to [22], researchers develop vaccination-related models to address various issues, such as determining the proportion of the population that needs to be immunised to eradicate the infectious agent and analysing the costs associated with implementing a mass vaccination programme. They also examine the implications if target coverage for eradication is not reached, assess the effects of waning vaccine-induced immunity, investigate the emergence of vaccine-resistant variants, and evaluate the role of booster doses in mitigating infections caused by mutations.

For example, [20] developed a model to assess the effect of vaccination on mortality and morbidity across age groups and to determine prioritisation strategies. In [17], the authors presented a method focused on allocating finite vaccine doses to minimise transmission. In [26], a mathematical model of COVID-19 transmission and vaccination was developed to fit reported mortality and excess mortality data in 185 countries, estimating the number of deaths that could have been averted had WHO vaccination coverage targets been met by the end of 2021. Similarly, [28] examined the impact of COVID-19 vaccines on the pandemic.

In [19], a model was proposed to understand UK epidemiological data and estimate vaccine efficacy, predicting the possible long-term dynamics of SARS-CoV-2 under a two-dose vaccination rollout and relaxation of non-pharmaceutical interventions (NPIs). This model estimated the basic reproduction number \mathcal{R}_0 and patterns of daily deaths and hospital admissions from January 2021 to January 2024. In [6], a model incorporating vaccination and treatment deduced that the critical vaccination threshold for eradication depends on vaccine efficacy.

Further, [22] introduced mass vaccination models predicting threshold coverage rates needed to eradicate infection, exploring vaccine-induced immunity waning over time, and examining interactions between vaccine-susceptible and vaccine-resistant strains. In [8], a model assessed vaccination programme impacts on transmission potential in large populations. [15] evaluated

vaccination's role in breaking transmission in South Africa, while [9] proposed a model indicating that an imperfect SARS vaccine could reduce the reproduction number below one to control outbreaks. [14] analysed COVID-19 infection dynamics with vaccination.

The authors of [2] investigated coronavirus dynamics in Saudi Arabia using a fractional-order vaccination model. [1] forecasted epidemic evolution during a vaccination campaign, while [23] used a compartmental model to advise on border restrictions during vaccine rollout. In [7], vaccination impacts on infection spread in Gauteng, South Africa were demonstrated, and [27] studied vaccination's impact on COVID-19 spread dynamics.

This study aims to understand the effects of vaccination rates and loss of protection on disease transmission. We present our model in Section 2, analyze its qualitative properties in Section 3, discuss results and simulations in Section 4, and conclude with key findings in Section 5.

2 Model description

We consider a population with homogeneous mixing, meaning all individuals have equal probability of contact with each other. The model comprises seven compartments representing different epidemiological states at time t :

- $S(t)$: Susceptible individuals
- $V(t)$: Vaccinated individuals
- $E(t)$: Exposed individuals
- $A(t)$: Asymptomatic infected individuals
- $I(t)$: Symptomatic infected individuals
- $H(t)$: Hospitalized individuals
- $P(t)$: Protected/recovered individuals

The total population is given by:

$$N(t) = S(t) + V(t) + E(t) + A(t) + I(t) + H(t) + P(t).$$

The system dynamics are governed by the following parameters:

- Π : Recruitment rate into the susceptible class
- β : Disease transmission rate
- ζ_1 : Probability of infection from asymptomatic contact
- ζ_2 : Probability of infection from symptomatic contact
- μ : Natural mortality rate (non-COVID-19)
- δ_1 : Rate from exposed to asymptomatic infectious
- δ_2 : Rate from exposed to symptomatic infectious

- α : Recovery rate of asymptomatic individuals
- ϵ : Recovery rate of symptomatic individuals
- γ : Hospitalization rate of symptomatic cases
- θ : COVID-19 mortality rate for symptomatic cases
- ω : COVID-19 mortality rate for hospitalized cases
- ν : Vaccination rate of susceptible individuals
- τ : Rate of vaccine-induced protection
- ρ : Rate of vaccine protection waning (return to susceptible)
- η : Recovery rate of hospitalized individuals

The force of infection λ is given by:

$$\lambda = \beta \left(\frac{\zeta_1 A}{N} + \frac{\zeta_2 I}{N} \right).$$

The compartmental transitions are illustrated in Figure 2.1 and governed by the following system of ordinary differential equations:

$$\left\{ \begin{array}{l} \frac{dS}{dt} = \Pi - \nu S - \lambda S - \mu S + \rho V, \\ \frac{dV}{dt} = \nu S - (\mu + \tau + \rho)V, \\ \frac{dE}{dt} = \lambda S - (\delta_1 + \delta_2 + \mu)E, \\ \frac{dA}{dt} = \delta_1 E - (\alpha + \mu)A, \\ \frac{dI}{dt} = \delta_2 E - (\gamma + \epsilon + \theta + \mu)I, \\ \frac{dH}{dt} = \gamma I - (\omega + \mu + \eta)H, \\ \frac{dP}{dt} = \alpha A + \epsilon I + \eta H + \tau V - \mu P. \end{array} \right. \quad (2.1)$$

The system (2.1) is solved subject to the initial conditions:

$$\left\{ \begin{array}{l} S(0) = S_0 > 0, \\ V(0) = V_0 \geq 0, \\ E(0) = E_0 \geq 0, \\ A(0) = A_0 \geq 0, \\ I(0) = I_0 \geq 0, \\ H(0) = H_0 \geq 0, \\ P(0) = P_0 \geq 0. \end{array} \right. \quad (2.2)$$

In the following section, we analyze the qualitative behavior of this system.

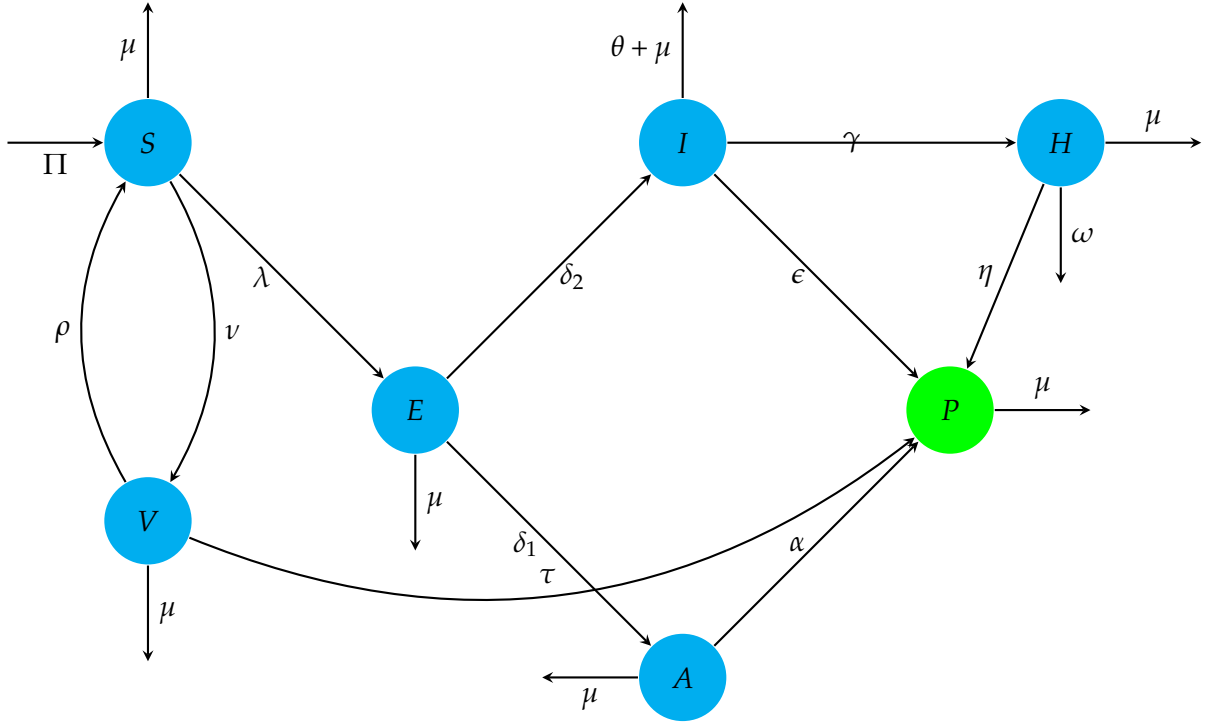


Figure 2.1: Flow diagram of the proposed SVEAIHP model

3 Model analysis

In this section, we focus on the qualitative properties of the system (2.1)(2.2), including the analysis of the invariant set and stability. We aim to gain insights into how the system behaves under various conditions and how it evolves over time.

3.1 Positivity and boundedness

In this context, the system pertains to populations; hence, we assume that all state variables are non-negative at time $t = 0$. Additionally, all model parameters are assumed to be non-negative. We define the set of all non-negative initial conditions satisfying a natural population bound. Let $\mathcal{U} \subset \mathbb{R}^7$ represent the feasible region.

$$\mathcal{U} = \left\{ (S, V, E, A, I, H, P) \in \mathbb{R}_+^7 \mid N \leq \frac{\Pi}{\mu} \right\}. \quad (3.1)$$

To establish the epidemiological significance of the model, it is crucial to demonstrate that each variable of the model, when initialized with positive conditions as outlined in Equation (2.2), remains non-negative for all time $t > 0$ within the feasible region described in equation (3.1).

3.1.1 Positivity of the solution

Using the initial conditions given in Equation (2.2), we demonstrate that the model's solutions $S(t)$, $V(t)$, $E(t)$, $A(t)$, $I(t)$, $H(t)$ and $P(t)$ are non-negative for all time $t > 0$.

Lemma 3.1 (Positivity of Solutions). *If the initial conditions satisfy $S(0) \geq 0$, $V(0) \geq 0$, $E(0) \geq 0$, $A(0) \geq 0$, $I(0) \geq 0$, $H(0) \geq 0$, and $P(0) \geq 0$, then the corresponding solutions $S(t)$, $V(t)$, $E(t)$, $A(t)$, $I(t)$, $H(t)$, and $P(t)$ of the system remain strictly positive for all time $t > 0$.*

Proof. Suppose, by contradiction, that the solution of the model (2.1) is not strictly positive for all $t \geq 0$. Then, there exists a first time $t^* > 0$ such that

$$t^* = \inf \{t \geq 0 \mid \min\{S(t), V(t), E(t), A(t), I(t), H(t), P(t)\} = 0\}.$$

Without loss of generality, assume $S(t^*) = 0$. By the definition of t^* , for all $t \in (0, t^*)$, we have $S(t) > 0$, $V(t) > 0$, $E(t) > 0$, $A(t) > 0$, $I(t) > 0$, $H(t) > 0$, $P(t) > 0$. Since $S(t)$ reaches zero at t^* from positive values, it attains a minimum at t^* . If $S(t)$ is differentiable at t^* , then

$$\left. \frac{dS}{dt} \right|_{t=t^*} \leq 0.$$

However, from the first equation in (2.1), we have

$$\frac{dS}{dt} = \Pi - \nu S - \lambda S - \mu S + \rho V.$$

At $t = t^*$, since $S(t^*) = 0$ and all parameters are positive, it follows that

$$\left. \frac{dS}{dt} \right|_{t=t^*} = \Pi > 0,$$

which contradicts the earlier deduction that $\left. \frac{dS}{dt} \right|_{t=t^*} \leq 0$. Hence, $S(t) > 0$ for all $t \geq 0$. By applying similar reasoning to $V(t)$, $E(t)$, $A(t)$, $I(t)$, $H(t)$, and $P(t)$, we conclude that all state variables remain strictly positive for all $t \geq 0$. Therefore, the solution of (2.1) remains in \mathbb{R}_+^7 for all $t \geq 0$. \square

3.1.2 The invariant region

We now establish that the solutions of the model (2.1) are bounded and remain in the positive orthant for all $t \geq 0$. To achieve this, we show that the biologically feasible region defined in (3.1) is positively invariant with respect to the dynamics of the system.

Lemma 3.2 (Boundedness and Invariant Region). *Let the initial conditions satisfy $S(0) \geq 0$, $V(0) \geq 0$, $E(0) \geq 0$, $A(0) \geq 0$, $I(0) \geq 0$, $H(0) \geq 0$, and $P(0) \geq 0$. Then the total population $N(t) = S(t) + V(t) + E(t) + A(t) + I(t) + H(t) + P(t)$ satisfies*

$$\limsup_{t \rightarrow \infty} N(t) \leq \frac{\Pi}{\mu}.$$

Moreover, the region

$$\mathcal{U} = \left\{ (S, V, E, A, I, H, P) \in \mathbb{R}_+^7 \mid N \leq \frac{\Pi}{\mu} \right\},$$

is positively invariant with respect to the dynamics of the system (2.1). That is, any solution starting in \mathcal{U} remains in \mathcal{U} for all $t \geq 0$.

Proof. Recall that the total human population is given by

$$N(t) = S(t) + V(t) + E(t) + A(t) + I(t) + H(t) + P(t).$$

Differentiating $N(t)$ along the solutions of the system yields

$$\frac{dN}{dt} = \Pi - \mu N - \theta I - \omega H.$$

Since all state variables are non-negative by the positivity result established in 3.1, and since $\theta, \omega > 0$, we observe that

$$\frac{dN}{dt} \leq \Pi - \mu N.$$

Now consider the comparison differential equation

$$\frac{dZ}{dt} = \Pi - \mu Z, \quad Z(0) = N_0.$$

The solution to this linear ODE is

$$Z(t) = \frac{\Pi}{\mu} (1 - e^{-\mu t}) + N_0 e^{-\mu t}.$$

Since $N(t) \leq Z(t)$ for all $t \geq 0$, it follows that

$$N(t) \leq \frac{\Pi}{\mu} (1 - e^{-\mu t}) + N_0 e^{-\mu t}.$$

Taking the limit as $t \rightarrow \infty$, we find

$$\limsup_{t \rightarrow \infty} N(t) \leq \frac{\Pi}{\mu}.$$

Therefore, all solutions of the model remain bounded above by $\frac{\Pi}{\mu}$, and since each compartment is non-negative, we conclude that the solutions remain in the set 3.1 for all $t \geq 0$. Hence, the region \mathcal{U} is positively invariant and attracting. In summary, the model is well-posed both mathematically and epidemiologically, and its solutions remain bounded and biologically meaningful within the region \mathcal{U} . \square

3.2 Equilibria and stability

In this section, we present the equilibrium points. We obtain the equilibrium points by setting the right-hand side of equations (2.1) to zero. We first find the disease-free equilibrium point. The disease-free equilibrium (DFE) is a point where there is no disease in the population, i.e., $E = A = I = H = 0$. The DFE point is given by $\varepsilon^0 = (S^0, V^0, 0, 0, 0, 0, P^0)$, where,

$$\begin{aligned} S^0 &= \frac{\Pi(\mu + \tau + \rho)}{\mu(\mu + \tau + \rho) + \nu(\mu + \tau)}, & V^0 &= \frac{\Pi\nu}{\mu(\mu + \tau + \rho) + \nu(\mu + \tau)}, \\ P^0 &= \frac{\Pi\tau\nu}{\mu((\mu(\mu + \tau + \rho) + \nu(\mu + \tau)))}. \end{aligned}$$

3.2.1 The basic reproduction number

To calculate the basic reproduction number, we use the next generation matrix as discussed by Van den Driessche and Watmough [25]. We set vector \mathcal{F} of rate of appearance of new infections from classes (E, A, I) and vector \mathcal{V} the net rate of transfer out of infected compartments.

$$\mathcal{F} = \begin{pmatrix} \lambda S \\ 0 \\ 0 \end{pmatrix}, \quad \mathcal{V} = \begin{pmatrix} (\delta_1 + \delta_2 + \mu)E \\ (\alpha + \mu)A - \delta_1 E \\ (\gamma + \epsilon + \theta + \mu)I - \delta_2 E \end{pmatrix}.$$

Computing the Jacobians of \mathcal{F} and \mathcal{V} at the DFE, we get

$$F = \begin{pmatrix} 0 & \beta S^* \cdot \frac{\zeta_1}{N^*} & \beta S^* \cdot \frac{\zeta_2}{N^*} \\ 0 & 0 & 0 \\ 0 & 0 & 0 \end{pmatrix}, \quad V = \begin{pmatrix} \delta_1 + \delta_2 + \mu & 0 & 0 \\ -\delta_1 & \alpha + \mu & 0 \\ -\delta_2 & 0 & \gamma + \epsilon + \theta + \mu \end{pmatrix}.$$

To calculate the basic reproduction number \mathcal{R}_0 , we seek the spectral radius of the next generation matrix $\mathcal{G} = FV^{-1}$. Hence, the expression for \mathcal{R}_0 . Let $a_1 = \delta_1 + \delta_2 + \mu$, $a_2 = \alpha + \mu$ and $a_3 = \gamma + \epsilon + \theta + \mu$. Then

$$V^{-1} = \begin{pmatrix} \frac{1}{a_1} & 0 & 0 \\ \frac{\delta_1}{a_1 a_2} & \frac{1}{a_2} & 0 \\ \frac{\delta_2}{a_1 a_3} & 0 & \frac{1}{a_3} \end{pmatrix} \Rightarrow FV^{-1} = \begin{pmatrix} \beta S^* \cdot \frac{1}{N^*} \left(\zeta_1 \cdot \frac{\delta_1}{a_1 a_2} + \zeta_2 \cdot \frac{\delta_2}{a_1 a_3} \right) & \frac{\beta S^*}{N^*} \zeta_1 \cdot \frac{1}{a_2} & \frac{\beta S^*}{N^*} \zeta_2 \cdot \frac{1}{a_3} \\ 0 & 0 & 0 \\ 0 & 0 & 0 \end{pmatrix}.$$

So the dominant eigenvalue is given by

$$\mathcal{R}_0 = \beta \cdot \kappa \cdot \left(\frac{\zeta_1 \cdot \delta_1}{(\delta_1 + \delta_2 + \mu)(\alpha + \mu)} + \frac{\zeta_2 \cdot \delta_2}{(\delta_1 + \delta_2 + \mu)(\gamma + \epsilon + \theta + \mu)} \right), \quad (3.2)$$

$$\text{where } \kappa = \frac{(\mu + \tau + \rho)}{\mu(\mu + \tau + \rho) + \nu(\mu + \tau)}. \quad (3.3)$$

The factor κ accounts for the effects of vaccination. The vaccination factor represents the proportion of the population that remains susceptible at the disease-free equilibrium. It captures how vaccination reduces the number of fully susceptible individuals. The factor incorporates the key parameters related to vaccination: the vaccination rate ν , vaccine-induced immunity τ , and the waning of vaccine protection ρ . The parameters are modulated by the natural death rate μ . When the vaccination rate ν increases, the proportion of susceptible individuals decreases, reflecting the protective effect of vaccination. Hence, this factor directly reduces the basic reproduction number \mathcal{R}_0 , quantifying the impact of vaccination on disease transmission. When no vaccination is implemented $\nu = 0$, the expression simplifies to $1/\mu$, indicating that the entire population is susceptible. Hence, the model without the vaccination compartment whose adjusted \mathcal{R}_0 is denoted as \mathcal{R}_0^{novac}

$$\mathcal{R}_0^{no\ vac} = \frac{\beta}{\mu} \cdot \left(\frac{\zeta_1 \cdot \delta_1}{(\delta_1 + \delta_2 + \mu)(\alpha + \mu)} + \frac{\zeta_2 \cdot \delta_2}{(\delta_1 + \delta_2 + \mu)(\gamma + \epsilon + \theta + \mu)} \right).$$

The basic reproduction number, \mathcal{R}_0 , is defined as the average number of secondary infections generated by a single infected individual introduced into a completely susceptible population during their life cycle. The basic reproduction number \mathcal{R}_0 indicates a threshold condition that the disease will be eradicated if $\mathcal{R}_0 < 1$; however, if $\mathcal{R}_0 > 1$, then the disease will persist. The disease-free equilibrium of the proposed models is locally asymptotically stable if $\mathcal{R}_0 < 1$. Biologically, this means that each infected individual produces, on average, fewer than one new infection, so the disease cannot sustain itself in the population.

3.2.2 Global stability of the disease-free equilibrium point

We study the global stability of the DFE using the method introduced by Castillo-Chavez *et al.* [4]. Consider a system of ordinary differential equations of the form

$$\begin{cases} \frac{dx}{dt} = F(x, Y), \\ \frac{dY}{dt} = G(x, Y), \quad G(x, 0) = 0, \end{cases}$$

where $x \in \mathbb{R}^3$ represents the uninfected classes and $Y \in \mathbb{R}^4$ denotes the number of infected individuals, which includes the exposed and the two infectious classes and the hospitalizations. $G(x, 0) = 0$, meaning that there is no infection when $Y = 0$. Let the point $\varepsilon^0 = (x^*, 0)$ denote the disease-free equilibrium point of the system (2.1) with 0 representing the zero vector and x^* denoting the steady-state value of the uninfected compartments when no disease is present.

Theorem 3.3 (Global Asymptotic Stability of DFE). *The disease-free equilibrium $\varepsilon^0 = (x^*, 0)$ is globally asymptotically stable in the biologically feasible region $\mathcal{U} \subset \mathbb{R}_+^{3+4}$ if the following two conditions are satisfied*

(H1) *The subsystem $\frac{dx}{dt} = F(x, 0)$ has x^* as a globally asymptotically stable equilibrium.*

(H2) *The function $G(x, Y)$ can be written in the form:*

$$G(x, Y) = AY - \hat{G}(x, Y), \quad \text{with } \hat{G}(x, Y) \geq 0 \text{ in } \mathcal{U},$$

where $A = \left. \frac{\partial G}{\partial Y} \right|_{(x^*, 0)}$ is a Metzler matrix (i.e., its off-diagonal entries are non-negative), and \mathcal{U} is the biologically meaningful region.

Moreover, this holds when the basic reproduction number satisfies $\mathcal{R}_0 < 1$.

Proof. First, we rewrite model (2.1) by partitioning into uninfected and infected compartments

$$x = (S, V, P)^\top \quad \text{and} \quad Y = (E, I, A, H)^\top.$$

Then, let the DFE be $\varepsilon^0 = (x^*, 0) = \left(\frac{\Pi(\mu+\tau+\rho)}{\mu(\mu+\tau+\rho)+\nu(\mu+\tau)}, \frac{\Pi\nu}{\mu(\mu+\tau+\rho)+\nu(\mu+\tau)}, \frac{\Pi\tau\nu}{\mu(\mu(\mu+\tau+\rho)+\nu(\mu+\tau))} \right)$ and the system $\frac{dx}{dt} = F(x, 0)$ becomes

$$\begin{cases} \frac{dS}{dt} = \Pi - (\nu + \mu)S + \rho V, \\ \frac{dV}{dt} = \nu S - (\mu + \tau + \rho)V, \\ \frac{dP}{dt} = \tau V - \mu P, \end{cases}$$

The condition H1 is satisfied. The system is linear and has a unique equilibrium, $x^* = (S^*, V^*, P^*)$. All the eigenvalues of the coefficient matrix have negative real parts; hence, the equilibrium x^* is globally asymptotically stable in the absence of infection. To examine H2, recall that the dynamics of the infected compartments are given by

$$\frac{dY}{dt} = G(x, Y) = AY - \hat{G}(x, Y),$$

where

$$A = \begin{pmatrix} -(\delta_1 + \delta_2 + \mu) & 0 & 0 & 0 \\ \delta_1 & -(\alpha + \mu) & 0 & 0 \\ \delta_2 & 0 & -(\gamma + \epsilon + \theta + \mu) & 0 \\ 0 & 0 & \gamma & -(\omega + \mu + \eta) \end{pmatrix},$$

is the Jacobian of G evaluated at the DFE, and

$$\hat{G}(x, Y) = \begin{pmatrix} \beta S \left(\frac{\zeta_1 I_1 + \zeta_2 I_2}{N} \right) \\ 0 \\ 0 \\ 0 \end{pmatrix} \geq 0,$$

for all $x, Y \in \mathcal{U}$, and all parameters and variables are non-negative. Since A is a Metzler matrix with strictly negative diagonal entries and $\hat{G}(x, Y) \geq 0$ in \mathcal{U} , condition (H2) is also satisfied. Therefore, we conclude that the disease-free equilibrium is globally asymptotically stable whenever $\mathcal{R}_0 < 1$. \square

The condition $\mathcal{R}_0 < 1$ plays a crucial role in ensuring that the disease-free equilibrium (DFE) is the only possible long-term behavior of the system.

3.2.3 Global stability of the endemic equilibrium point

In this section, we consider the endemic equilibrium point of the system (2.1). The endemic equilibrium is a point in the system at which the disease persists within a population. For an endemic equilibrium point $(S^*, V^*, E^*, A^*, I^*, H^*, P^*)$ to exist, at least one of E^* or A^* or I^* must be nonzero. To find the endemic equilibrium point, we assume that $E(t) \neq 0, A(t) \neq 0, I(t) \neq 0, H(t) \neq 0$, hence, $\varepsilon^* = (S^*, V^*, E^*, A^*, I^*, H^*, P^*)^T$. We solve the system

$$\begin{cases} \Pi - \nu S^* - \lambda^* S^* - \mu S^* + \rho V^* = 0, \\ \nu S^* - (\mu + \tau + \rho) V^* = 0, \\ \lambda S^* + -(\delta_1 + \delta_2 + \mu) E^* = 0, \\ \delta_1 E^* - (\alpha + \mu) A^* = 0, \\ \delta_2 E^* + (\gamma + \epsilon + \theta + \mu) I^* = 0, \\ \gamma I^* - (\omega + \mu + \eta) H^* = 0 \\ \alpha A^* + \epsilon I^* + \eta H^* + \tau V^* - \mu P^* = 0. \end{cases} \quad (3.4)$$

where

$$\lambda^* = \frac{\beta \zeta_1 A^*}{N} + \frac{\beta \zeta_2 I^*}{N}. \quad (3.5)$$

and using the expression for \mathcal{R}_0 we obtain

$$\begin{cases} S^* = \frac{(\mu + \tau + \rho) \Pi}{(\mu(\mu + \tau + \rho) + \nu(\mu + \tau)) \mathcal{R}_0}, \\ V^* = \frac{\nu \Pi}{(\mu(\mu + \tau + \rho) + \nu(\mu + \tau)) \mathcal{R}_0}, \\ E^* = \frac{\Pi(\mathcal{R}_0 - 1)}{(\delta_1 + \delta_2 + \mu) \mathcal{R}_0}, \\ A^* = \frac{\Pi \delta_1 (\mathcal{R}_0 - 1)}{(\alpha + \mu)(\delta_1 + \delta_2 + \mu) \mathcal{R}_0}, \\ I^* = \frac{\Pi \delta_2 (\mathcal{R}_0 - 1)}{(\gamma + \epsilon + \theta + \mu)(\delta_1 + \delta_2 + \mu) \mathcal{R}_0}, \\ H^* = \frac{\gamma \Pi \delta_2 (\mathcal{R}_0 - 1)}{(\eta + \mu + \omega)(\gamma + \epsilon + \theta + \mu)(\delta_1 + \delta_2 + \mu) \mathcal{R}_0}, \\ P^* = \frac{\alpha A^* + \epsilon I^* + \eta H^* + \tau V^*}{\mu}. \end{cases} \quad (3.6)$$

From the third, fourth and fifth equations of (3.6), we notice that the biologically meaningful endemic equilibrium state exists if and only if $\mathcal{R}_0 > 1$. We claim and prove that endemic equilibrium point is globally asymptotical stable.

Theorem 3.4. *The COVID-19 model (2.1) has a unique positive endemic equilibrium whenever $\mathcal{R}_0 > 1$, which is globally asymptotically stable.*

Proof. Consider the following Lyapunov function:

$$L(S, V, E, A, I, H) = (S - S^* \ln S) + (V - V^* \ln V) + a_1 (E - E^* \ln E) + a_2 (A - A^* \ln A) + a_3 (I - I^* \ln I) + a_4 (H - H^* \ln H), \quad (3.7)$$

where a_1, a_2, a_3 and a_4 are non-negative constants to be determined. By differentiating (3.7) we obtain

$$\begin{aligned} \frac{dL(t)}{dt} = & \left(1 - \frac{S^*}{S}\right) \frac{dS}{dt} + \left(1 - \frac{V^*}{V}\right) \frac{dV}{dt} + a_1 \left(1 - \frac{E^*}{E}\right) \frac{dE}{dt} + a_2 \left(1 - \frac{A^*}{A}\right) \frac{dA}{dt} + a_3 \left(1 - \frac{I^*}{I}\right) \frac{dI}{dt} \\ & + a_4 \left(1 - \frac{H^*}{H}\right) \frac{dH}{dt}. \end{aligned} \quad (3.8)$$

Substituting (2.1) we get

$$\begin{aligned} \frac{dL(t)}{dt} = & \left(1 - \frac{S^*}{S}\right) (\Pi - \nu S - \lambda S - \mu S + \rho V) + \left(1 - \frac{V^*}{V}\right) (\nu S - (\mu + \tau + \rho)V) \\ & + a_1 \left(1 - \frac{E^*}{E}\right) (\lambda S - (\delta_1 + \delta_2 + \mu)E) + a_2 \left(1 - \frac{A^*}{A}\right) (\delta_1 E - (\alpha + \mu)A) \\ & + a_3 \left(1 - \frac{I^*}{I}\right) (\delta_2 E - (\gamma + \epsilon + \theta + \mu)I) + a_4 \left(1 - \frac{H^*}{H}\right) (\gamma I - (\omega + \mu + \eta)H) \\ = & [\Pi - \nu S - \lambda S - \mu S + \rho V] + \left[-\Pi \frac{S^*}{S} + (\nu + \mu) S^* + \lambda S^* - \rho V \frac{S^*}{S}\right] \\ & + [\nu S - (\mu + \tau + \rho)V] + \left[-\nu S \frac{V^*}{V} + (\mu + \tau + \rho)V^*\right] + a_1 [\lambda S - (\delta_1 + \delta_2 + \mu)E] \\ & + a_1 \left[-\lambda S \frac{E^*}{E} + (\delta_1 + \delta_2 + \mu)E^*\right] + a_2 [\delta_1 E - (\alpha + \mu)A] \\ & + a_2 \left[-\delta_1 E \frac{A^*}{A} - (\alpha + \mu)A^*\right] + a_3 [\delta_2 E - (\gamma + \epsilon + \theta + \mu)I] \\ & + a_3 \left[-\delta_2 E \frac{I^*}{I} + (\gamma + \epsilon + \theta + \mu)I^*\right] + a_4 [\gamma I - (\omega + \mu + \eta)H] + a_4 \left[-\gamma I \frac{H^*}{H} + (\omega + \mu + \eta)H^*\right]. \end{aligned} \quad (3.9)$$

Re-arranging, we obtain

$$\begin{aligned} \frac{dL(t)}{dt} = & [\Pi + (\nu + \mu) S^* + (\tau + \rho + \mu) V^* + a_1 (\delta_1 + \delta_2 + \mu) E^* + a_2 (\alpha + \mu) A^* + a_3 (\gamma + \epsilon + \theta + \mu) I^* \\ & + a_4 (\eta + \omega + \mu) H^*] - \mu S - \frac{\beta \zeta_1 AS}{N} - \frac{\beta \zeta_2 IS}{N} \\ & + \rho V - \Pi \frac{S^*}{S} + \frac{\beta \zeta_1 AS^*}{N} + \frac{\beta \zeta_2 IS^*}{N} - \rho V \frac{S^*}{S} - (\tau + \rho + \mu) V - \nu S \frac{V^*}{V} + a_1 \frac{\beta \zeta_1 AS}{N} \\ & + a_1 \frac{\beta \zeta_2 IS}{N} - a_1 (\delta_1 + \delta_2 + \mu) E + a_1 \frac{\beta \zeta_1 ASE^*}{NE} + a_1 \frac{\beta \zeta_2 ISE^*}{NE} + a_2 \delta_1 E - a_2 (\alpha + \mu) A \\ & - a_2 \delta_1 \frac{A^*}{A} + a_3 \delta_2 E - a_3 (\gamma + \epsilon + \theta + \mu) I - a_3 \delta_2 \frac{I^*}{I} + a_4 \gamma I - a_4 (\eta + \omega + \mu) H - a_4 \gamma \frac{H^*}{H} \\ = & C - C_1(h, u, w, x, y, z). \end{aligned} \quad (3.10)$$

For simplicity of notation, denote $w = \frac{S}{S^*}$, $x = \frac{V}{V^*}$, $u = \frac{E}{E^*}$, $z = \frac{A}{A^*}$, $y = \frac{I}{I^*}$, $h = \frac{H}{H^*}$, let $C = \Pi + (\nu + \mu) S^* + (\tau + \rho + \mu) V^* + a_1 (\delta_1 + \delta_2 + \mu) E^* + a_2 (\alpha + \mu) A^* + a_3 (\gamma + \epsilon + \theta + \mu) I^* + a_4 (\eta + \omega + \mu) H^*$. Then we rewrite (3.10) as

$$\begin{aligned} \frac{dL(t)}{dt} = & C - \mu S^* w - \frac{\beta \zeta_1 A^* S^* w z}{N} - \frac{\beta \zeta_2 I^* S^* w y}{N} + \rho V^* x - \Pi \frac{1}{w} + \frac{\beta \zeta_1 A^* S^* z}{N} + \frac{\beta \zeta_2 I^* S^* y}{N} - \rho V^* \frac{x}{w} \\ & - (\tau + \rho + \mu) V^* x - \nu S^* \frac{w}{x} + a_1 \frac{\beta \zeta_1 A^* S^* w z}{N} + a_1 \frac{\beta \zeta_2 I^* S^* w y}{N} - a_1 (\delta_1 + \delta_2 + \mu) E^* u \\ & + a_1 \frac{\beta \zeta_1 A^* S^* w z}{N u} + a_1 \frac{\beta \zeta_2 I^* S^*}{N u} + a_2 \delta_1 E^* u - a_2 (\alpha + \mu) A^* z - a_2 \delta_1 \frac{1}{z} + a_3 \delta_2 E^* u \\ & - a_3 (\gamma + \epsilon + \theta + \mu) I^* y - a_3 \delta_2 \frac{1}{y} + a_4 \gamma I^* y - a_4 (\eta + \omega + \mu) H^* h - a_4 \gamma \frac{1}{h}. \end{aligned} \quad (3.11)$$

We want to choose the suitable constants $a_i \leq 0$ for $(i = 1, 2, 3, 4)$ so that the derivative of the function $L(S, V, E, A, I, H)$ is negative definite or semi-definite. We follow the method used in [16] and rewrite the derivative of function $L(S, V, E, A, I, H)$ with constants $a_i > 0$ ($i = 1, 2, 3, 4$) in the following form

$$\sum_{k=1}^K d_k (n_k - g_{k,1} - g_{k,2} - \cdots - g_{k,n_k}), \quad (3.12)$$

where $d_k \geq 0$, $(k = 1, 2, \dots, K)$, $g_{k,i}$, is an expression only including multiplication and division of elements in the set Γ such that the product of $g_{k,i}$ s is unity. We define a set Γ of by

$$\Gamma = \left\{ h, u, w, x, y, z, yw, wz, \frac{u}{y}, \frac{u}{z}, \frac{1}{w}, \frac{x}{w}, \frac{w}{x}, \frac{y}{h}, \frac{wy}{u}, \frac{wz}{u} \right\},$$

such that we have a total of five cases,

$$\left\{ w, \frac{1}{w} \right\}, \left\{ \frac{1}{w}, \frac{w}{x}, x \right\}, \left\{ \frac{1}{w}, \frac{wz}{u}, \frac{u}{z} \right\}, \left\{ \frac{1}{w}, \frac{u}{y}, \frac{yw}{u} \right\}, \left\{ \frac{x}{w}, \frac{w}{x} \right\}.$$

We rewrite expression (3.12) as

$$d_1 \left(2 - w - \frac{1}{w} \right) + d_2 \left(2 - \frac{x}{w} - \frac{w}{x} \right) + d_3 \left(3 - \frac{1}{w} - \frac{w}{x} - x \right) + d_4 \left(3 - \frac{1}{w} - \frac{wz}{u} - \frac{u}{z} \right) + d_5 \left(3 - \frac{1}{w} - \frac{u}{y} - \frac{yw}{u} \right). \quad (3.13)$$

Suppose the right-hand side of (3.11) is equal to (3.13). We then equate the coefficients of like

terms of these two expressions to obtain the following

$$\left\{ \begin{array}{l} d_1 = +\mu S^*, \\ d_2 = \rho V^*, \\ d_3 = (\mu + \tau) V^*, \\ d_4 = a_1 \frac{\beta \epsilon_1 A^* S^*}{N} = a_2 \delta_1 E^*, \\ d_5 = a_1 \frac{\beta \epsilon_1 I^* S^*}{N} = a_3 \delta_2 E^*, \\ d_1 + d_3 + d_4 + d_5 = \Pi, \\ d_1 + d_2 + d_3 + d_4 + d_5 = C, \\ d_2 + d_3 = \nu S^*, \\ 1 - a_1 = 0, \\ a_2 (\alpha + \mu) = \frac{\beta \epsilon_1 S^*}{N}, \\ a_3 (\gamma + \epsilon + \theta + \mu) = a_4 \gamma + \frac{\beta \epsilon_2 S^*}{N}, \\ (\delta_1 + \delta_2 + \mu) = a_2 \delta_1 + a_3 \delta_2, \\ a_4 \gamma I^* = 0. \end{array} \right. \quad (3.14)$$

Using the relationships given by

$$\left\{ \begin{array}{l} \Pi = \nu S^* + \lambda^* S^* + \mu S^* - \rho V^*, \\ \nu S^* = (\mu + \tau + \rho) V^*, \\ \lambda^* S^* = (\delta_1 + \delta_2 + \mu) E^*, \\ \delta_1 E^* = (\alpha + \mu) A^*, \\ \delta_2 E^* = (\gamma + \epsilon + \theta + \mu) I^*, \\ \gamma I^* = (\omega + \mu + \eta) H^*, \end{array} \right. \quad (3.15)$$

we obtain that

$$a_1 = 1, \quad a_2 = \frac{\beta \zeta_1 S^*}{N} \frac{1}{(\alpha + \mu)} = \frac{\beta \zeta_1 A^* S^*}{N \delta_1 E^*}, \quad a_3 = \frac{\beta \zeta_2 S^*}{N} \frac{1}{(\gamma + \epsilon + \theta + \mu)} = \frac{\beta \zeta_2 I^* S^*}{N \delta_2 E^*}, \quad a_4 = 0,$$

and hence

$$d_1 = \mu S^*, \quad d_2 = \rho V^*, \quad d_3 = (\mu + \tau) V^*, \quad d_4 = \frac{\beta \zeta_1 A^* S^*}{N}, \quad d_5 = \frac{\beta \zeta_2 I^* S^*}{N}.$$

This yields the derivative of $L(S, V, E, A, I, H)$ as

$$\begin{aligned} \frac{dL(t)}{dt} &= \mu S^* \left(2 - w - \frac{1}{w} \right) + \rho V^* \left(2 - \frac{x}{w} - \frac{w}{x} \right) + (\mu + \tau) V^* \left(3 - \frac{1}{w} - \frac{w}{x} - x \right) \\ &\quad + \frac{\beta \zeta_1 A^* S^*}{N} \left(3 - \frac{1}{w} - \frac{wz}{u} - \frac{u}{z} \right) + \frac{\beta \zeta_2 I^* S^*}{N} \left(3 - \frac{1}{w} - \frac{u}{y} - \frac{yw}{u} \right) \\ &\leq 0. \end{aligned}$$

Note that $\frac{dL(t)}{dt} = 0$ when $S^* = S, V^* = V, E^* = E, A^* = A, I^* = I, H^* = H$. Consequently, we obtain by LaSalle's invariance principle ϵ^* is globally asymptotically stable. This completes the proof. \square

Table 4.1: A table showing the estimated parameter values used in model (2.1)

Symbol	Parameter description	Value	Source
Π	Recruitment into the susceptible class	$\mu N_0 = 653 \text{ day}^{-1}$	standard
μ	death rate	$\frac{1}{61 \times 365} \text{ day}^{-1}$	standard
ν	Rate of vaccination	0.025 day^{-1}	fitted
τ	Fully protected individuals progressing to protected class P class	$1/7 \text{ day}^{-1}$	fitted
ρ	rate of losing protection	0.03 day^{-1}	fitted
β	transmission rate	0.98	fitted
ζ_1	Probability of infection through contact with asymptomatic individuals	0.95	fitted
ζ_2	Probability of infection through contact with symptomatic individuals	0.93	fitted
δ_1	Rate of progression from E to A	$1/6 \text{ day}^{-1}$	fitted
δ_2	Rate of progression from E to I	$1/2 \text{ day}^{-1}$	fitted
α	Progression from asymptomatic class to protected class	$1/8 \text{ day}^{-1}$	fitted
ϵ	Progression from symptomatic to Protected class	$1/8 \text{ day}^{-1}$	fitted
γ	Progression from symptomatic I to hospitalized H	$1/7 \text{ day}^{-1}$	fitted
θ	COVID-19 induced death rate from I class	0.1 day^{-1}	fitted
η	Rate of progression from H to protected class P class	0.1 day^{-1}	fitted
ω	COVID-19 induced death rate from H class	$1/9 \text{ day}^{-1}$	fitted

In this section, we investigated the qualitative nature of model (2.1). We proceed to the next section, where we estimate parameters, check their sensitivity with respect to the reproduction number \mathcal{R}_0 , and perform simulations to understand the impact of our target parameters on mitigating COVID-19.

4 Results analysis and discussion

4.1 Model validation

We fit the developed model to data to authenticate our model. We use the data for the new cases of COVID-19 recorded between 14 February 2021 and 24 October 2021. The data was extracted from [18]. To fit the model to the data, we adopt the Maximum Likelihood estimation (MLE) algorithm implemented in the fitR package. The results of our fit are shown in Figure 4.1, where the black dots represent the data points for weekly new cases of COVID-19 infections reported, and the red solid line is the model output. Table 4.1 shows the estimated values for the parameters used in model (2.1).

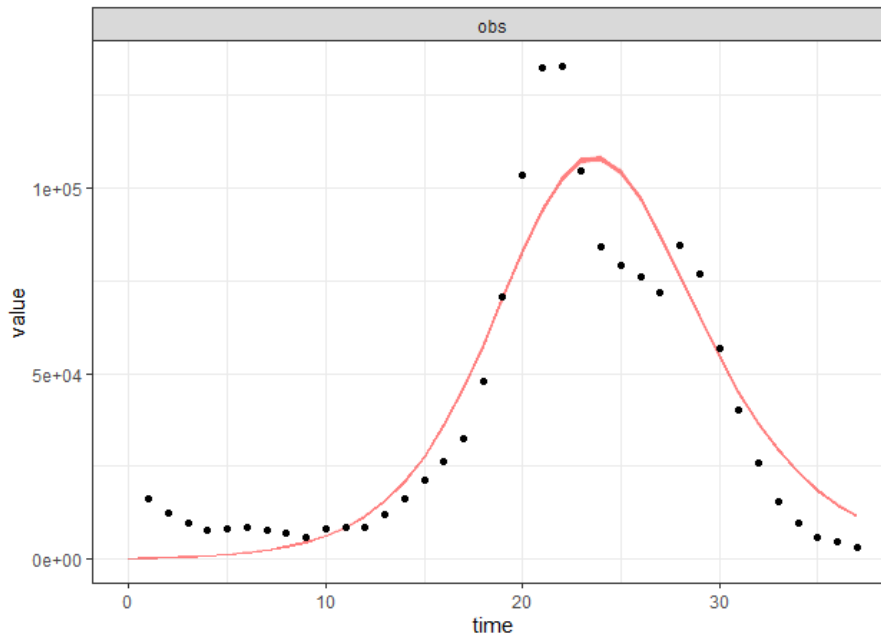


Figure 4.1: A figure showing the model fitted to the data between 14 February 2021 and 24 October 2021 of the COVID-19 pandemic in South Africa. The black-dotted line represents the reported data for COVID-19 positive cases, whereas the red-continuous line shows the goodness of fit. Parameter values used are as listed in Table (4.1) with reporting estimated to be 13%.

4.2 Sensitivity analysis

We use sensitivity analysis to identify where we can improve our model performance and design by identifying influential parameters and offering information regarding their quantitative relationship with the model output. The parameters targeted in our research are those bringing gain in the vaccinated class, and also those that create losses in the same class. But some other factors are more important to \mathcal{R}_0 than the ones we are studying in this model. For instance, the parameter β has the strongest positive correlation with \mathcal{R}_0 , but we will not dwell on it much as we seek to identify how vaccination parameters manipulate the \mathcal{R}_0 . Note that, when proposing intervention strategies to obtain the optimized results, it is advantageous to target all influential parameters for manipulation in the introduction of intervention strategies. This information is crucial for both the design of the model and data assimilation and for reducing nonlinear complex models. We used the normalized forward sensitivity indices of \mathcal{R}_0 to identify the influential models and used PRCC to quantify these findings as shown in 4.2. A parameter with a positive index increases the value of \mathcal{R}_0 when it is increased, while a parameter with a negative index decreases the value of \mathcal{R}_0 whenever it is increased.

The sensitivity analysis results indicate that increasing the following model parameters would increase disease transmission potential: the probability of transmission β , the mortality rate μ , the rate of susceptibility of vaccinated individuals ρ , the rate at which individuals move from the exposed class to the asymptomatic class, δ_1 , the rate at which hospitalized individuals recover is η , and the disease transmission rates from asymptomatic and symptomatic individuals are ζ_1 and ζ_2 . On the other hand, increasing the following model parameters may reduce disease burden: (i) rate of progression from asymptomatic class to recovered α ; (ii)

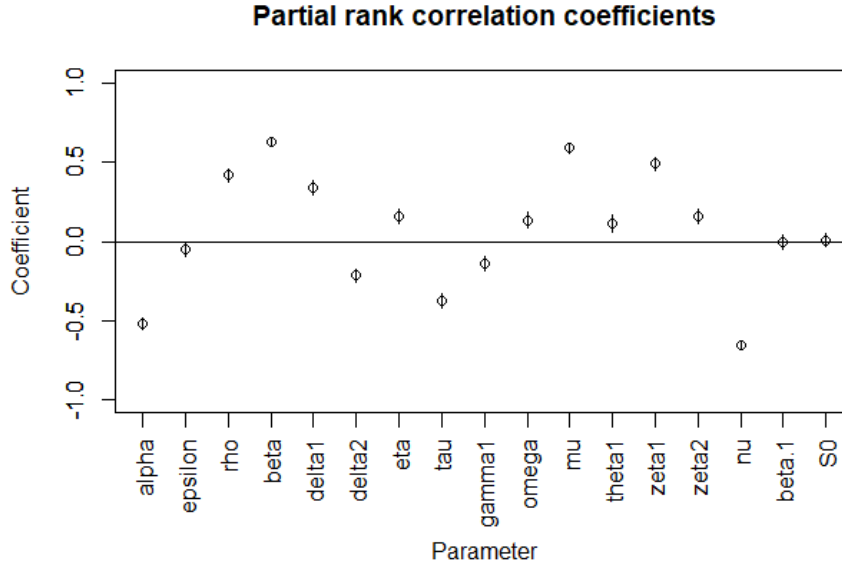


Figure 4.2: Sensitivity analysis of \mathcal{R}_0 to the model parameters.

transition from exposed to symptomatic infectious class δ_2 ; (iii) progression from vaccinated class to protected class τ ; and (iv) rate of vaccination of individuals ν .

We aim to mainly understand the impact of vaccination. This understanding will help us develop more effective public health strategies. In the next section, we focus on parameters involved in the vaccination class and vary them to observe how they influence the spread of COVID-19 in the population. We examine different scenarios to understand the influence of a combination of controlling these parameters.

4.3 Model simulations and discussion

We performed numerical simulations of our proposed model to visualize the parameters that most significantly influence the system's behavior. Overall, simulations show that vaccines are useful in reducing the risk of COVID-19 infection. We use the following initial conditions $S = 59893884$, $V = 22260$, $E = 14245$, $A = 17850$, $I = 16363$, $H = 3922$, $M = 93540$. We first analyze the parameter ν , which shows a strong negative correlation with the basic reproduction number, as noted in 4.2. Figure 4.3 illustrates the impact of the rate of vaccination ν on the asymptomatic cases (A), exposed cases (E), hospitalized cases (H), and symptomatic cases (I). In our simulations, we vary ν with the values 0.09, 0.1, 0.15, and 0.3. We observed that a sufficiently high vaccination rate can significantly reduce the number of cases in all four compartments.

Vaccinated individuals will gain vaccine-induced protection at the rate of (τ), thereby progressing to the protected compartment. We performed simulations to understand the effect of the parameter τ , which informs us of the vaccine's ability to protect individuals from infection. Figure 4.4 shows how the four groups in the model (2.1) change when we adjust the vaccination rate ν and the vaccine's effectiveness τ . Looking at Figure 4.4, we see that with a faster protection rate of $\tau = 1/7$, which means it takes an average of 7 days to be fully protected, the peaks are a bit lower than with a slower protection rate of $\tau = 1/28$. The differ-

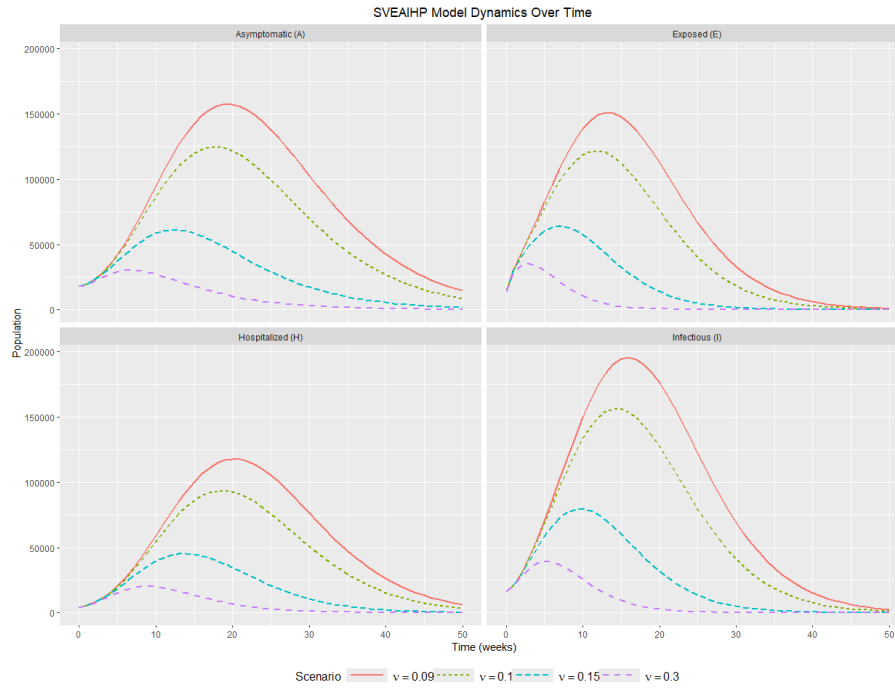


Figure 4.3: Effect of vaccination rate, $v = [0.09, 0.10, 0.15, 0.30]$.

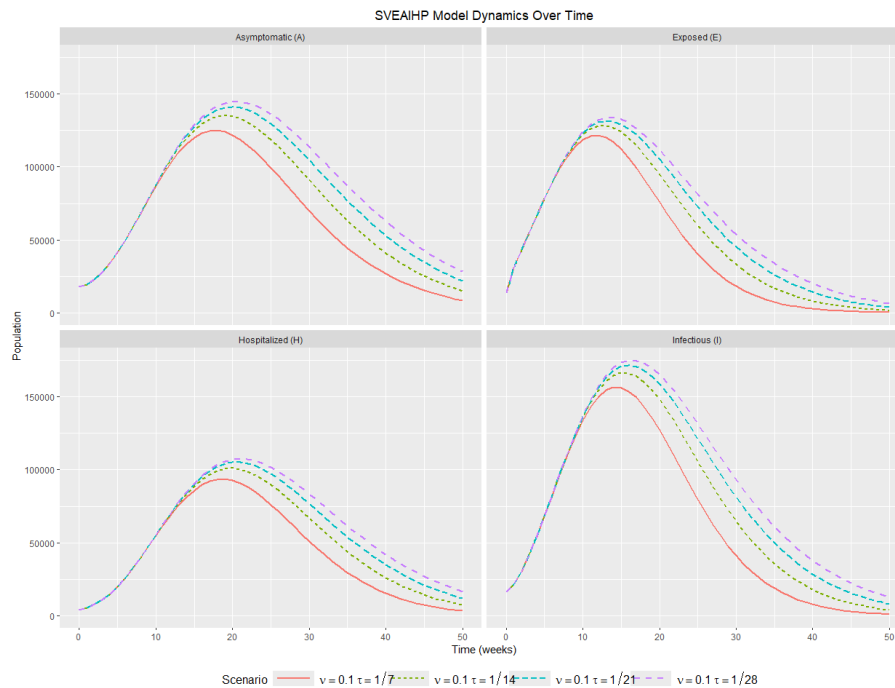


Figure 4.4: Effect of low vaccination rate ($v = 0.10$) and time to full protection ($\tau = [1/7, 1/14, 1/21, 1/28]$).

ences between τ values are relatively small compared to the differences between v values (see Figure 4.5). Vaccination rate v has a much stronger impact than the rate of gaining protection τ . Increasing the vaccination rate is more effective in reducing peak infections than worrying

about the rate of full protection. However, varying τ shows that improvements will suffice when τ is moved from extremely slow $\tau = 1/28$ to moderate $\tau = 1/14$ protection development. However trajectories do not differ much. This is observed in the sensitivity analysis

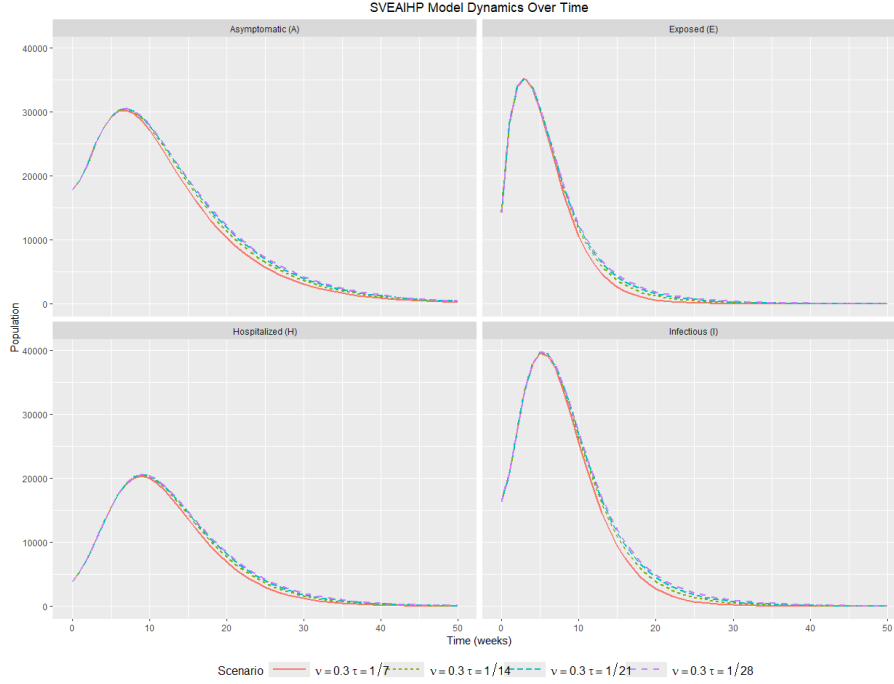


Figure 4.5: Effect of high vaccination rate ($\nu = 0.30$) and time to full protection ($\tau = [1/7, 1/14, 1/21, 1/28]$).

where the parameter τ has a weak negative correlation with \mathcal{R}_0 . Figure 4.5 demonstrates the trajectory of four of the seven classes of model (2.1) when the measure of vaccination is increased to $\nu = 0.3$ and the measure of vaccine protection τ values are varied as before. The simulations reveals that when the vaccination rate is high, the number of infections will be reduced, however, the rate at which the vaccine will confer protection does not significantly affect the trajectories when the vaccination rate is kept constant. Hence, improving the rate at which the vaccine confers protection may not necessarily improve the control strategy, but increasing the rate of vaccination may help to control the disease. The trajectories we observe as a result of varying the factor τ remain close to each other, meaning that this parameter does not significantly impact the time taken to reach the disease-free equilibrium if the vaccination rate remains constant.

We further simulate the vaccination rate ν against the rate at which the vaccinated become susceptible ρ . The trajectories from the simulation are observed in Figure 4.6. We observe the impact of a low vaccination rate, for instance, $\nu = 0.15$. The results indicate that the rate at which the vaccinated individuals lose protection and become susceptible again increases the number of in the exposed E , asymptomatic A , symptomatic I and hospitalized H classes. For instance, when the vaccinated individuals lose protection in seven days, the infections are surge. We examine the simulations in Figure 4.6 when the vaccination rate is low, $\nu = 0.1$. In all compartments A, E, H , and I , a faster loss of protection $\rho = 1/30$ exhibits noticeably higher peaks. Much lower peaks are seen for slower loss of protection $\rho = 1/120$. The higher vaccination rate $\nu = 0.30$ shown in Figure 4.7 results in lower peak values in all compartments

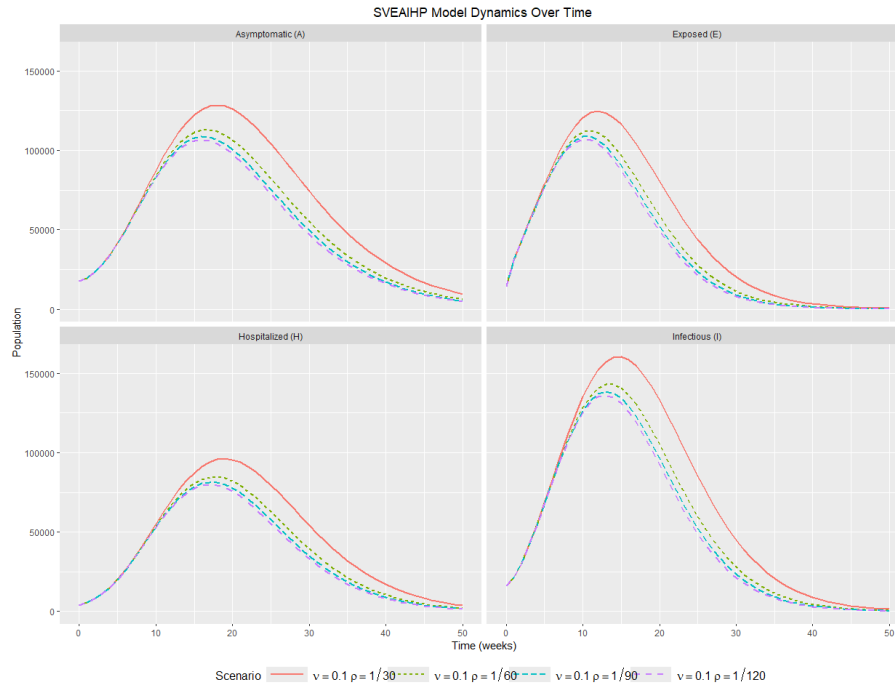


Figure 4.6: Effect of low vaccination rate ($\nu = 0.10$) and time to loss of protection ($\rho = [1/30, 1/60, 1/90, 1/120]$).

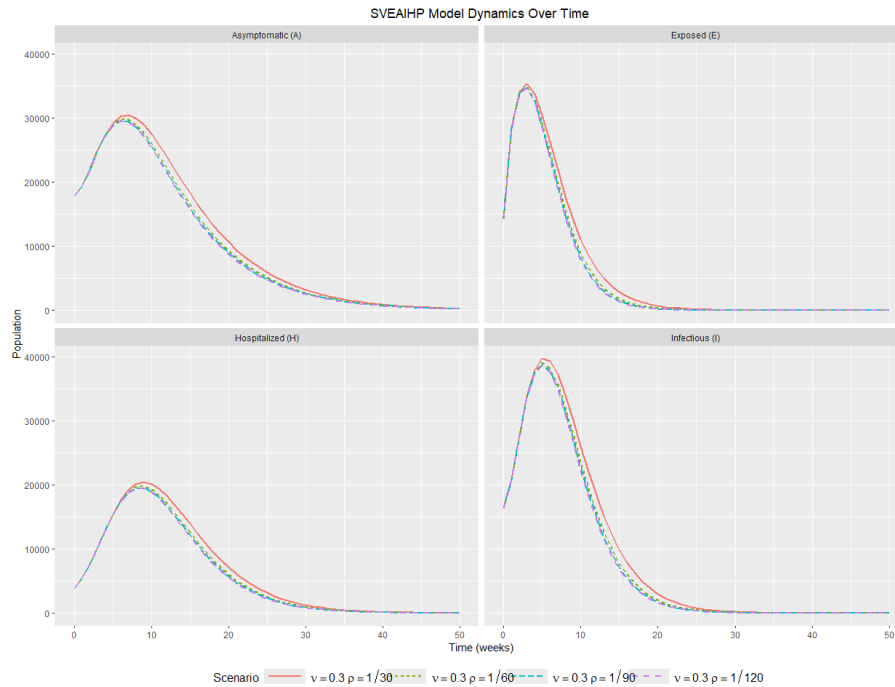


Figure 4.7: Effect of high vaccination rate ($\nu = 0.30$) and time to loss of protection ($\rho = [1/30, 1/60, 1/90, 1/120]$). The high rate of vaccination offsets the impact of the rate at which the vaccinated lose protection.

compared to the plot with $\nu = 0.1$. Peaks are reduced by about 50%. The difference in

the trajectories due to loss of protection in Figure 4.7 is not as noticeable as it is at lower vaccination rates in Figure 4.6. In both scenarios, a rapid loss of protection with $\rho = 1/30$ results in higher peaks. Trajectories for slower loss rates $\rho = 1/60, 1/90, 1/120$ in Figure 4.7 are remarkably similar, with few deviations. Thus, high vaccination coverage reduces the effect of protection durability, countering the damage caused by the loss of the vaccine's protectiveness. We observe that when a vaccine takes less time to wane, it means more individuals will be protected. Hence, there will be fewer susceptible individuals, and in turn, this reduces the exposed and the infectious.

The analysis of the parameters ν , ρ , and τ has revealed the influence played by these parameters in considering vaccination as a control strategy. The most important parameter in consideration is the rate of vaccination. But it's vital to study how quickly the vaccinated become vulnerable before they are fully protected from the virus. Rate of protection loss ρ has strong effects, possibly even greater than that of the vaccination rate when the vaccination rate is too low. Regardless of the vaccination rate, rapid loss of protection $\rho = 30$ days significantly worsens the epidemic. However, long-lasting protection $\rho = 120$ days significantly reduces the size of an epidemic. Over time, a high vaccination rate becomes crucial in safeguarding the population against the effects of protection loss. When the vaccination coverage is high, the returns for protection durability decrease.

Where high vaccination coverage is not possible, durability of the vaccine and coverage should be given equal weight in vaccine development. However, a successful approach would be a combination of high vaccination rates and long-lasting protection. When $\nu = 0.1, \rho = 120$ days, we observe moderate peaks. At $\nu = 0.30, \rho = 30$ days, we observe slightly lower peaks, but the lowest peaks occur when $\nu = 0.30, \rho = 120$ days. This demonstrates that the main factor influencing the success of epidemic control is vaccination rate. The biggest benefit comes from attaining high ν , so prioritize vaccination coverage first. However, in low vaccination coverage, protection durability is also important, i.e., at low ν , ρ becomes crucial. we emphasise that durability is less important at high coverage. The best result is achieved with practical feasibility when high coverage and reasonable durability are combined.

5 Conclusion

We formulated a deterministic mathematical model to investigate the impact of vaccination on the disease dynamics of COVID-19. We calculated the disease-free equilibrium and computed the basic reproduction number. We quantified the impact of vaccination. We calculated the basic reproduction number $\mathcal{R}_0 = 4.8$ without vaccination; however, when we included vaccination, the basic reproduction number became $\mathcal{R}_0 = 2.2$. This agrees with the theoretical findings that the vaccination factor κ reduces the reproduction number. Sensitivity analysis of the basic reproduction number was carried out, and it was established that parameters ν , β , and μ were key in the reduction of COVID-19.

Our model aimed to understand the impact of vaccination; hence, we mainly focused on three parameters related to vaccination: ν , ρ , and τ . The simulation results reveal that the vaccination rate is key to controlling COVID-19. However, we established that identifying an optimum vaccination rate will be ideal in the control of COVID-19 infections through vaccination. However, where resources are a limiting factor, it is important to also understand the rate at which the population loses protection after vaccination. A faster rate of loss of protection will negate the impact of vaccination. A deeper dive into the impacts of the specific vaccines could have given a clearer picture of the performance of the different parameters. A

study like this can be useful for policymakers in determining the rate at which vaccines can be administered to the target population, and in determining the choice of vaccine to consider whenever vaccines may have different specifications.

Declarations

Funding

The research of K.C.P. contained in this paper was supported by the South African National Research Foundation.

Conflict of interest

The authors have no conflicts of interest to declare.

References

- [1] M. ANGELI, G. NEOFOTISTOS, M. MATTHEAKIS, AND E. KAXIRAS, *Modelling the effect of the vaccination campaign on the COVID-19 pandemic*, *Chaos, Solitons & Fractals*, **154** (2022), 111621. [DOI](#)
- [2] A.-Y. ASMA, M. AFZAAL, M.-H. DARASSI, M.-A. KHAN, M.-Y. ALSHAHRANI, M.-A. SULIMAN, *Mathematical Model of Vaccinations Using New Fractional Order Derivative*, *Vaccines*, **10**(12) (2022), 1980. [DOI](#)
- [3] C. V. CARDEMIL, C. YI, C.-M. POSAVAD, M.-L. BADELL, K. BUNGE, M.-J. MULLIGAN, L. PARAMESWARAN ET AL., *Maternal COVID-19 Vaccination and Prevention of Symptomatic Infection in Infants*, *Pediatrics*, **153**(3) (2024), e2023064252. [DOI](#)
- [4] C. CASTILLO-CHAVEZ, Z. FENG AND W. HUANG, *On the Computation of \mathcal{R}_0 and its Role on Global Stability*, *Mathematical Approaches for Emerging and Reemerging Infectious Diseases: An Introduction*, **2002**(1) (2002), 229–250. [DOI](#)
- [5] A. CHRISTIE, S. HENLEY, F. LINDA, ET AL., *Decreases in COVID-19 Cases, Emergency Department Visits, Hospital Admissions, and Deaths Among Older Adults Following the Introduction of the COVID-19 Vaccine United States, September 6, 2020 May 1, 2021*, *Morbidity and Mortality Weekly Report*, **70**(23) (2021), 858–864. [DOI](#)
- [6] M.-L. DIAGNE, H. RWEZAURA, S. TCHOUMI AND J. TCHUENCHE, *A Mathematical Model of COVID-19 with Vaccination and Treatment*, *Computational and Mathematical Methods in Medicine*, **2021**(1) (2021), 1250129. [DOI](#)
- [7] C.-J. ELDHOLM, B. LEVY, L. SPENCE, ET AL., *A vaccination model for COVID-19 in Gauteng, South Africa*, *Infectious Disease Modelling*, **7**(3) (2022), 333–345. [DOI](#)
- [8] C.-P. FARRINGTON, *On vaccine efficacy and reproduction numbers*, *Mathematical Biosciences*, **185**(1) (2003), 89–109. [DOI](#)
- [9] A. B. GUMEL, C. C. MCCLUSKEY AND J. WATMOUGH, *An SVEIR Model for Assessing Potential Impact of an Imperfect Anti-SARS Vaccine*, *Mathematical Biosciences and Engineering*, **3**(3) (2006), 485–512. [DOI](#)

- [10] E-J. HAAS, F-J. ANGULO, J. McLAUGHLIN ET AL., *Impact and effectiveness of mRNA BNT162b2 vaccine against SARS-CoV-2 infections and COVID-19 cases, hospitalizations, and deaths following a nationwide vaccination campaign in Israel: an observational study using national surveillance data*, *The Lancet*, **397**(10287) (2021), 1819–1829. DOI
- [11] N. HALASA, S. OLSON, M. STAAT, ET AL, ET AL., *Effectiveness of Maternal Vaccination with mRNA COVID-19 Vaccine During Pregnancy Against COVID-19 Associated Hospitalization in Infants Aged <6 Months 17 States, July 2021January 2022, Morbidity and Mortality Weekly Report*, **71**(7) (2022), 264–270. DOI
- [12] Y. HALIM, N. TOUAFEK AND Y. YAZLIK, *Dynamic behavior of a second-order nonlinear rational difference equation*, *Turkish Journal of Mathematics*, **39**(6) (2015), 1004–1018. DOI
- [13] G. JANA, G. BAJPAI, P-T. OCAK ET AL., *Virus-Induced Acute Respiratory Distress Syndrome Causes Cardiomyopathy Through Eliciting Inflammatory Responses in the Heart*, *Circulation*, **150**(1) (2024), 49–61. DOI
- [14] S-A-A. KARIM (ed.), *Intelligent Systems Modeling and Simulation II: Machine Learning, Neural Networks, Efficient Numerical Algorithm and Statistical Methods*, Springer Nature, **444** (2022). DOI
- [15] M. KINYILI, J. B. MUNYAKAZI AND A. Y. A. MUKHTAR, *Assessing the impact of vaccination on COVID-19 in South Africa using mathematical modeling*, *Applied Mathematics & Information Sciences*, **15**(6) (2021), 701–716. DOI
- [16] J. LI, Y. XIAO, F. ZHANG AND Y. YANG, *An algebraic approach to proving the global stability of a class of epidemic models*, *Nonlinear Analysis: Real World Applications*, **13**(5) (2012), 2006–2016. DOI
- [17] J. LIU AND X. SHANG, *Computational Epidemiology*, Springer International Publishing, 2020. DOI
- [18] E. MATHIEU, H. RITCHIE, L. RODÉS-GUIRAO ET AL., *Coronavirus Pandemic (COVID-19)*, OurWorldInData.org, 2024. URL
- [19] S. MOORE, E. HILL, M. TILDESLEY, D. LOUISE AND M. KEELING, *Vaccination and non-pharmaceutical interventions for COVID-19: a mathematical modelling study*, *The Lancet. Infectious Diseases*, **21** (2021), 793–802. DOI
- [20] N. NURAINI, K-K. SUKANDAR, P. HADISOEMARTO ET AL., *Mathematical models for assessing vaccination scenarios in several provinces in Indonesia*, *Infectious Disease Modelling*, **6** (2021), 1236–1258. DOI
- [21] P. RZYMSKI, N. KASIANCHUK, D. SIKORA AND B. PONIEDZIAEK, *COVID19 vaccinations and rates of infections, hospitalizations, ICU admissions, and deaths in Europe during SARSCoV2 Omicron wave in the first quarter of 2022*, *Journal of Medical Virology*, **95**(1) (2022), e28131. DOI
- [22] A. SCHERER AND A. McLEAN, *Mathematical models of vaccination*, *British Medical Bulletin*, **62**(1) (2002), 187–199. DOI
- [23] N. STEYN, M. J. PLANK, R. N. BINNY ET AL., *A COVID-19 model for Aotearoa New Zealand*, *Scientific Reports*, **12**(1) (2022), 2270. DOI

- [24] A. SUMMAN AND A. NANDI, *Timing of non-pharmaceutical interventions to mitigate COVID-19 transmission and their effects on mobility: a cross-country analysis*, The European Journal of Health Economics, **23** (2022), 105–117. [DOI](#)
- [25] P. VAN DEN DRIESSCHE AND J. WATMOUGH, *Reproduction numbers and sub-threshold endemic equilibria for compartmental models of disease transmission*, Mathematical Biosciences, **180**(1–2) (2002), 29–48. [DOI](#)
- [26] O. J. WATSON, G. BARNSLEY, J. TOOR, A. B. HOGAN, P. WINSKILL AND A. C. GHANI, *Global impact of the first year of COVID-19 vaccination: a mathematical modelling study*, The Lancet Infectious Diseases, **22**(9) (2022), 1293–1302. [DOI](#)
- [27] B. YANG, Z. YU AND Y. CAI, *The impact of vaccination on the spread of COVID-19: Studied by a mathematical model*, Physica A: Statistical Mechanics and its Applications, **590** (2022), 126717. [DOI](#)
- [28] M. YAVUZ, F. Ö. COAR, F. GÜNAY AND F. ÖZDEMİR, *A New Mathematical Modeling of the COVID-19 Pandemic Including the Vaccination Campaign*, Open Journal of Modelling and Simulation, **9**(3) (2021), 299–321. [DOI](#)
- [29] World Health Organization (WHO), *Weekly Epidemiological Update on COVID-19, Edition 166*, 2024. [URL](#)